TEMPERATURE STRESSES IN EARLY AGE CONCRETE DUE TO HYDRATION

Mats Emborg, MSc
Stig Bernander, Associate Professor
Division of Structural Engineering,
Luleå University of Technology, Luleå

ABSTRACT

Theoretical models for the analysis of thermal induced stresses in massive concrete structures are presented. Laboratory tests are conducted in order to calibrate the theoretical models for different types of cement, concrete mixtures etc.

Keywords: Mass concrete, thermal stresses, young concrete, creep functions, cracking

1. INTRODUCTION

In concrete structures a temperature rise occurs in hardening from the hydration process. The structure then strives to expand. However, restraints of different kinds often prevent this expansion. Compressive and tensile stresses are hence induced in the structure. It is often of primary interest to prevent the tensile stresses to reach such magnitudes that cracking takes place. This is especially important in massive concrete structures such as thick walls and dams.

At the Luleå University of Technology a project is undertaken, in which the above thermally induced stresses are studied both analytically and experimentally. In this paper basic theoretically predicted stresses and test results show that it is essential that an appropriate creep function is adopted. This must be calibrated to the specific type of concrete considered.

2. THEORETICAL MODELS FOR CALCULATION OF THERMALLY INDUCED STRESSES

2.1 General

The most important parameters in an analysis of thermally induced stresses in a massive concrete structure are the thermal properties, the creep properties, and the restraint to which the structure is subjected.

Thermal properties are important characteristics of mass concrete. Large dimensions may imply a nearly adiabatic temperature rise due to hydration. The temperature rise is therefore significant and takes place over a long period of time. In a massive concrete structure the temperature distribution will also be nonuniform. In the calculation of the evolution of the temperature due to hydration, several parameters must be considered. These parameters include the following: type of cement and aggregate, type of concrete mixture, mix temperature, dimensions of the structure, temperature in the surrounding air and in adjoining structures.

Creep properties of young concrete are often disregarded in the analysis of thermal stresses. A typical behaviour of stress and strain in early age creep is the age-dependence shown in Fig 2.1. In a thermal stress analysis there are also nonlinear creep effects, caused by high stress levels. High stress levels may occur in several stages in the hardening process of a concrete structure. Although there are many creep models described in literature, only a few can be considered to be valid for early age creep in concrete.

The third parameter, the restraint, is of two types. The first type is the internal restraint, which occurs inside the massive and statically highly indeterminate structure itself (internal indeterminancy). This is the case, for example, when the structure is subjected to a nonuniform temperature field, see fig 2.2a. Nonuniform drying of the concrete can also lead to internal restraint. The second type of restraint arises from the hyperstatic

connection of the structure to surrounding structures (external indeterminancy). Here we must model for instance the friction or adhesion to a basement and the stiffness of an earlier cast section, see Fig 2.2b.

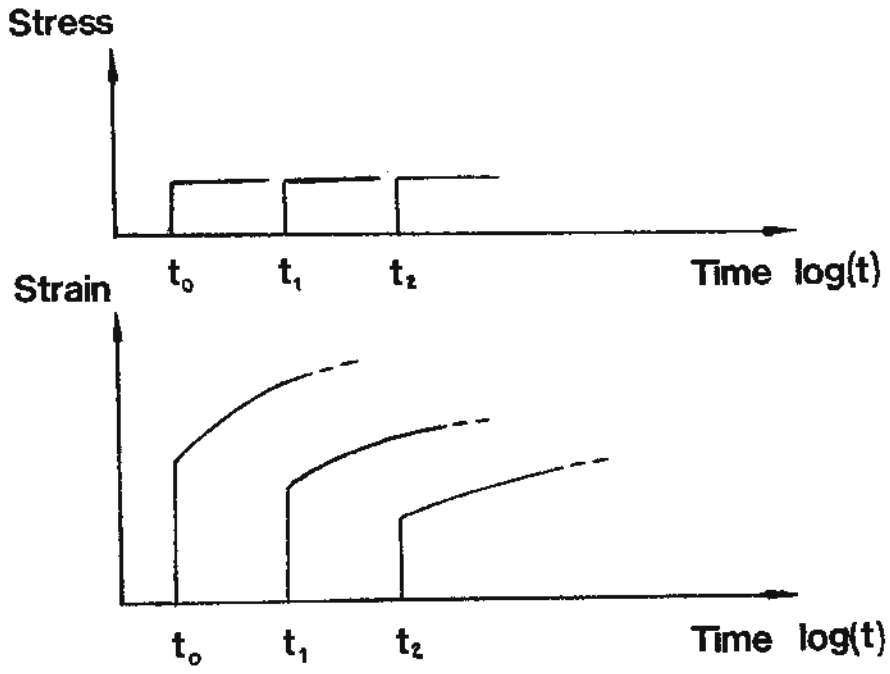

Fig 2.1 Age-dependence in early age concrete creep.

It can be seen from the discussion above that a complete analysis would be very complicated. In order to formulate a realistic but from a practical point of view applicable mathematical model it is therefore necessary to introduce some simplifications. In this paper the following assumptions are made:

(a) The effect of drying is neglected.

(b) The temperature is assumed to be uniformly distributed except of course when the effect of nonuniform internal temperature distribution is studied. In this report only stresses caused by an average temperature rise in a section are treated.

(c) The effect of the nonlinearity in creep due to high stress levels that may arise is neglected in some of the used creep models.

(d) The structure is assumed to be surrounded by inflexible supports, i.e. the restraint is 100 per cent.

In the following two theories for calculation of the thermal stresses are described: the creep compliance method and the creep coefficient method.

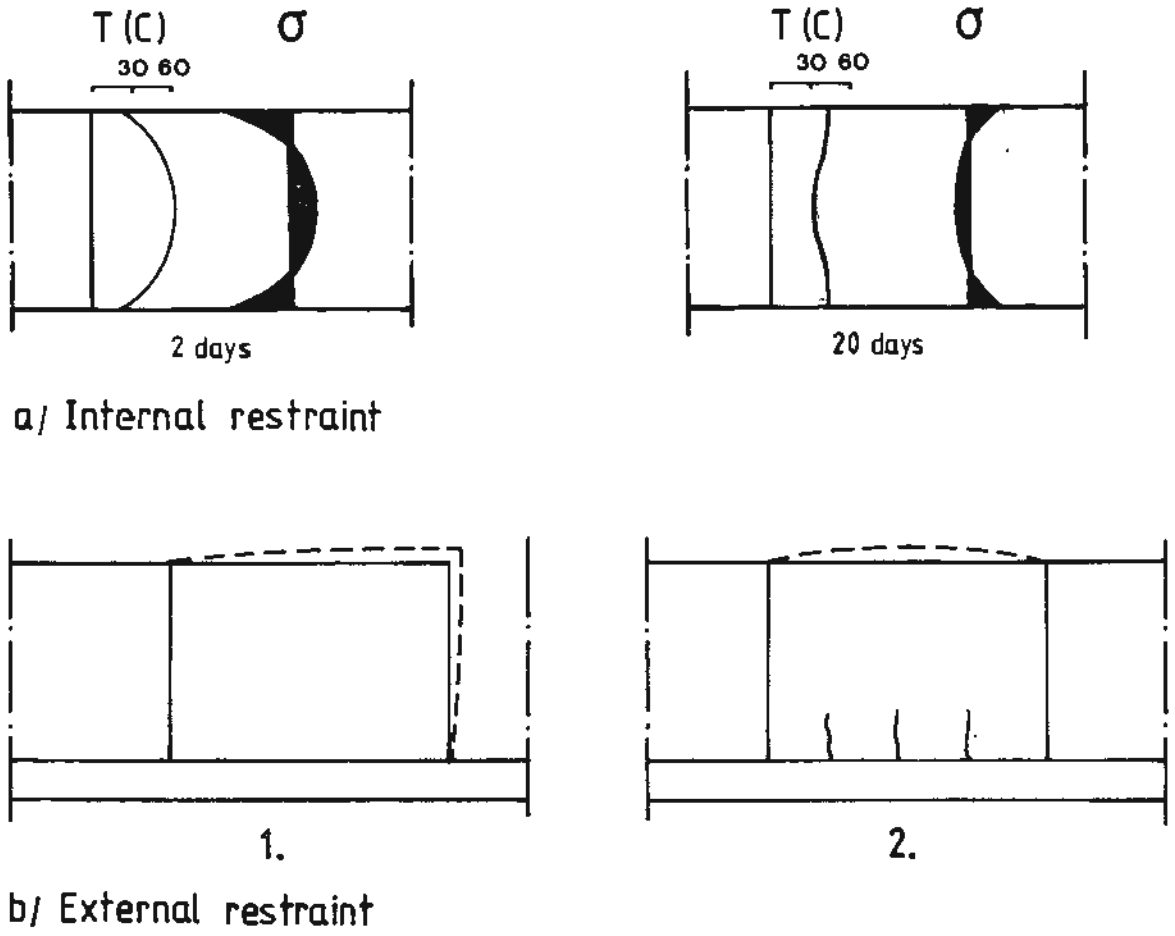

Fig 2.2 Conditions of restraint in massive concrete structures:
a) Internal restraint in a wall section caused by a non-uniform temperature field. Compressive stresses and tensile stresses occur both in the center of the wall and at the surface.
b) External restraint conditions: A massive concrete wall cast on a slab. The dashed lines mark schematically the temperature induced deformation. In comparison with case 1, case 2 involves a higher degree of restraint and cracks occur as shown in the figure.

2.2 Creep compliance method

In the creep compliance method the time dependent deformation at time t, $\varepsilon(t)$, from a loading at time t', $\sigma(t')$, is modelled by the compliance function $J(t,t')$ (see also Fig 2.3a).

$$\varepsilon(t) = J(t,t') \cdot \sigma(t') \tag{2.1}$$

According to the prinicple of superposition a linear integral-type viscoelastic law with such compliance functions may be used to describe the temperature induced deformations in the concrete. In this manner, the strain history, $\varepsilon(t)$, induced by an arbitrary stress history, $\sigma(t)$, can be written /5/

$$\varepsilon(t) = \int_{o}^{t} J(t,t')\, d\sigma(t') + \varepsilon^{o}(t) \tag{2.2}$$

where $J(t,t')$ is the creep compliance at time t for the loading time t'

$d\sigma(t')$ is the stress increment at time t', see also Fig 2.3b

ε^{o} is the stress-independent strain at time t, for example thermal strain or shrinkage.

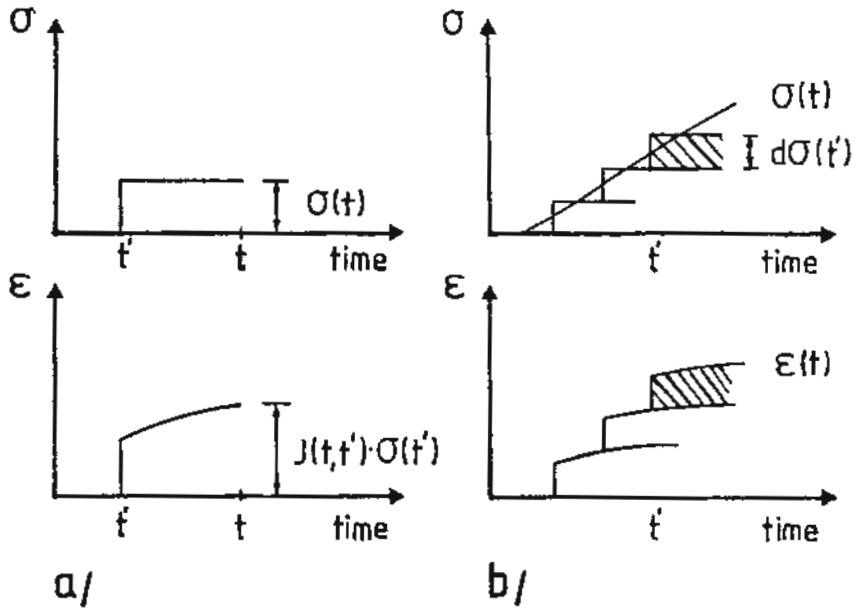

Fig 2.3 a) Time-dependent deformation at time t, $\varepsilon(t)$, from a loading at time t', $\sigma(t')$ b) Superimposed viscoelastic deformation, $\varepsilon(t)$, from a given stress history.

A multiaxial generalization of Eq (2.2) can be obtained by assuming isotropy. In this case the stress-strain relation can be written in the same form as for the uniaxial case if stress and strain are resolved into their volumetric and deviatoric components /5/.

$$3\varepsilon^{V}(t) = \int_{o}^{t} J^{V}(t,t')\, d\sigma^{V}(t') + 3\varepsilon^{o}(t) \qquad (2.3a)$$

$$2\varepsilon^{D}_{ij}(t) = \int_{o}^{t} J^{D}(t,t')\, d\sigma^{D}_{ij}(t') \qquad (2.3b)$$

where $\varepsilon^{V}(t) = \varepsilon_{kk}(t)/3$ is the volumetric strain

$\sigma^{V}(t) = \sigma_{kk}(t)/3$ is the volumetric stress

$\varepsilon^{o}(t)$ is the stress independent strain, thermal strain, shrinkage etc.

$\varepsilon^{D}_{ij}(t) = \varepsilon_{ij}(t) - \delta_{ij}\varepsilon^{V}(t)$ are the deviatoric strains $(i,j, = 1, 2, 3)$

$\sigma^{D}_{ij}(t) = \sigma_{ij}(t) - \delta_{ij}\sigma^{V}(t)$ are the deviatoric stresses $(i,j, = 1, 2, 3)$

δ_{ij} is the Kroneckers delta, = 1 for $i = j$ and = 0 for $i \neq j$.

The functions $J^{V}(t,t')$ and $J^{D}(t,t')$ are the volumetric and deviatoric compliance functions, which are related to the creep compliance as follows

$$J^{V}(t,t') = 6(\tfrac{1}{2} - \nu)\, J(t,t') \qquad (2.4a)$$

$$J^{D}(t,t') = 2(1 + \nu)\, J(t,t') \qquad (2.4b)$$

where the Creep Poisson ratio, ν, is assumed to have a constant value $\simeq 0.18$ /5/.

Theoretical treatments of the creep compliance, J(t,t'), can be found in the literature. In the calculation of uniaxial thermal stresses with Eq (2.3) conducted at Luleå University of Technology /1/, formulae for J(t,t') proposed by Bazant /6/ and Wilson /7/ were used. Results obtained from these calculations are shown in section 2.4.

2.3 Creep coefficient method

In the creep coefficient method, the deformation at time t induced by loading at time t' is subdivided into two parts. The first part is the elastic, instantaneous deformation, $\varepsilon_{el}(t')$, and the second part is the inelastic, viscous, deformation, $\varepsilon_v(t,t')$. The total deformation, $\varepsilon_{tot}(t,t')$ can then be written (see also Fig 2.4)

$$\varepsilon_{tot}(t,t') = \varepsilon_{el}(t') + \varepsilon_v(t,t') \tag{2.5}$$

The elastic deformation $\varepsilon_{el}(t')$ can be written in the form

$$\varepsilon_{el}(t') = \frac{\sigma(t')}{E(t')} \tag{2.6}$$

where $\sigma(t')$ is the stress applied at time t'
$E(t')$ is the modulus of elasticity at time t'.

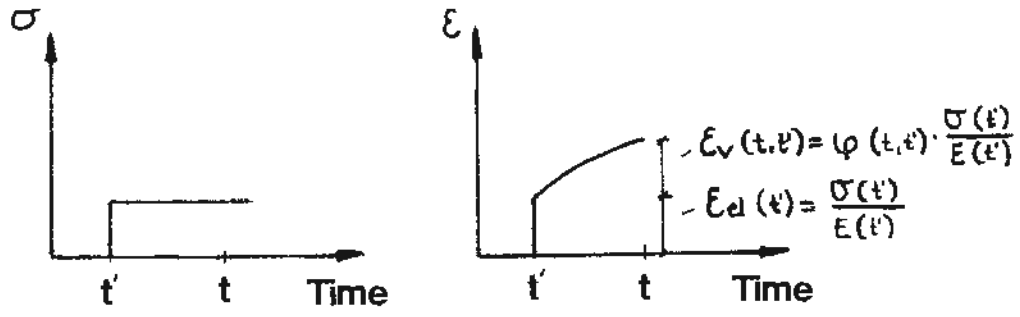

Fig 2.4 Elastic and creep deformation at time t for loading at t'.

The viscous deformation (the creep) at time t for a concrete loaded at time t', is related to the elastic part by the creep function $\varphi(t,t')$, commonly called the "creep coefficient".

$$\varepsilon_v(t,t') = \varphi(t,t') \cdot \varepsilon_{el}(t') \tag{2.7}$$

A substitution of the expressions for $\varepsilon_{el}(t')$ and $\varepsilon_v(t,t')$ given by Eqs (2.6) and (2.7) into Eq (2.5) yields an often used creep law

$$\varepsilon_{tot}(t,t') = \frac{\sigma(t')}{E(t')} \left(1 + \varphi(t,t')\right) \tag{2.8}$$

The time-derivate of the total strain ε_{tot} in Eq (2.8) is a rather complicated expression. Assuming a time hardening material implies several simplifications and the time-derivative can then be written (according to Dischinger /10/):

$$\frac{d\varepsilon_{tot}(t)}{dt} = \frac{\sigma(t)}{E_o} \frac{d\varphi(t)}{dt} + \frac{1}{E_o} \frac{d\sigma(t)}{dt} \tag{2.9}$$

where $\sigma(t)$ is the stress at time t

$\frac{d\varphi(t)}{dt}$ and $\frac{d\sigma(t)}{dt}$ are the time-derivative of the creep coefficient and of stress

E_o is the modulus of elasticity, here assumed to have a constant value.

Eq (2.9) implies that the creep functions $\varphi_a(t)$ and $\varphi_b(t)$ (Fig 2.5b), induced by stresses σ_o and $\Delta\sigma$ (Fig 2.5a), are parallel. As an illustration to Eq (2.9), Fig 2.5c shows the time-dependent strain increase, $\Delta\varepsilon(t)$, during the time interval between t_1 and t_2.

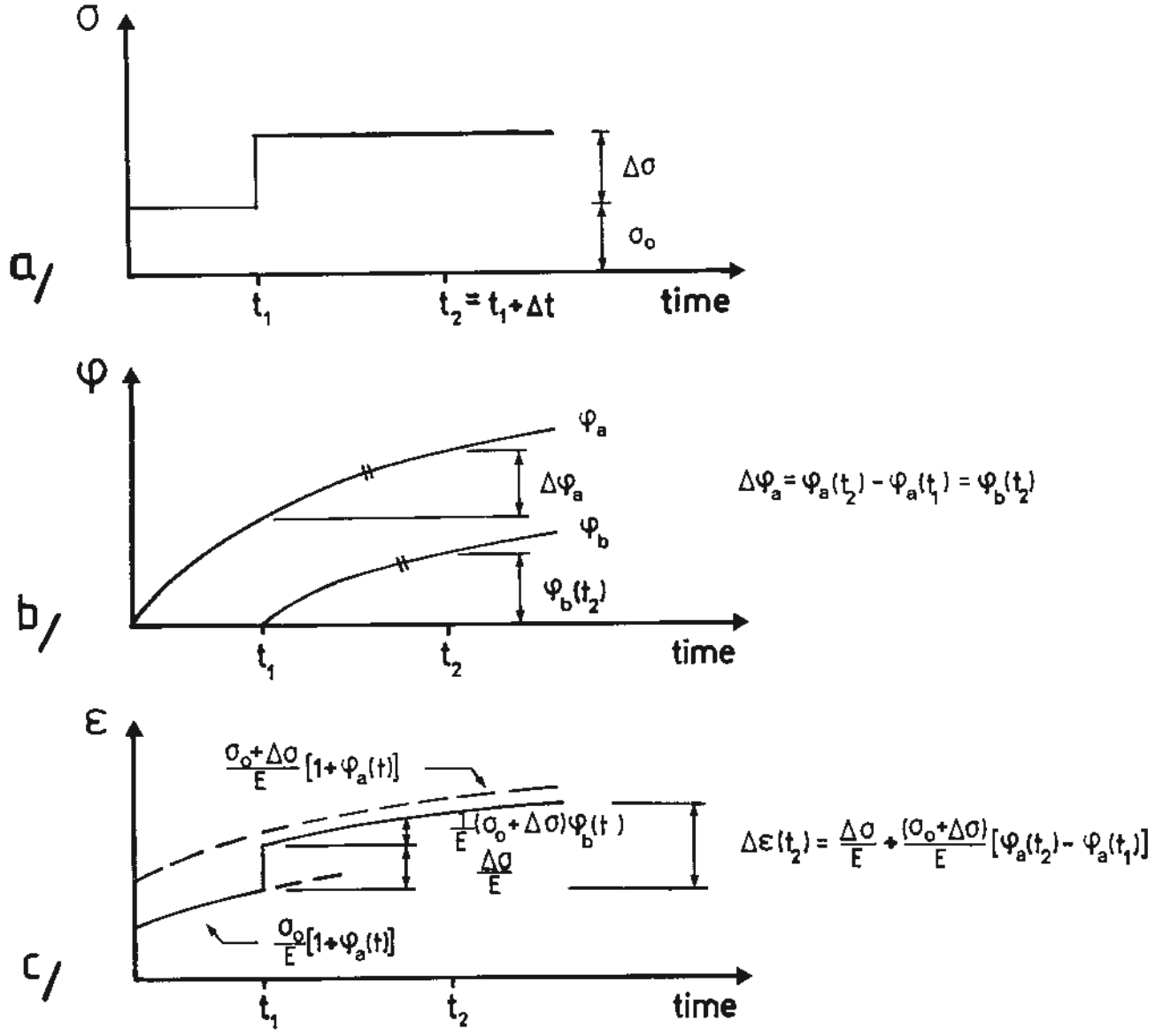

Fig 2.5 Time hardening material. a) Increase of stress level at time t_1. b) Parallel creep functions for stresses σ_o and $\Delta\sigma$. c) Time-dependent strain increase, $\Delta\varepsilon$, induced by the stress increment.

In Eq (2.9) the E-modulus is assumed to be constant. However, this is not the case for young concrete where a considerable increase of the value of E-modulus occur. To compensate for this Eq (2.9) has been modified to

$$d\varepsilon_{tot}(t) = \frac{\sigma(t)}{E(t)}\, d\varphi(t) + \frac{d\sigma(t)}{E(t)} - \frac{\sigma(t)\, dE(t)}{(E(t))^2} \qquad (2.11)$$

in which $d\varepsilon_{tot}(t)$ is the total strain increment at time t

$E(t)$ and $\sigma(t)$ are the Young's modulus and stress at time t

$dE(t)$ and $d\sigma(t)$ are the corresponding increments of the Young's modulus and the stress during the time dt

$d\varphi(t)$ is the increment of the creep coefficient during the time dt.

Compared to Eq (2.9) the following changes have been made. E_o has been changed to $E(t)$ in the first two terms. To compensate for the reduction in flexibility the third term has been introduced.

Criticism can be directed towards the assumption of time-hardening. It leads to an underestimation of the creep caused by stresses applied some time after the initial loading. However, the assumption of time hardening has found a wide use in the literature [5], [11] and [12],and for that reason we have used it here in order to obtain a comparison with the creep compliance method.

Eq (2.11) is a differential equation which is valid for the calculation of uniaxial thermal stresses in concrete.

If the temperature strain increment, $\alpha dT(t)$, is introduced in the term $d\varepsilon_{tot}(t)$, the stress increment $d\sigma(t)$ is obtained. For instance at 100 % restraint, i.e. for rigid supports, $d\varepsilon_{tot}(t) = \alpha dT(t)$.

With Eq (2.11), discretized for finite difference calculations, computation of uniaxial thermal stresses were performed /1/. In the calculations the change of creep coefficient, $d\varphi(t)$, was obtained from theoretical work on the creep of concrete, presented in literature. Formulae for the creep coefficient, according to Bernander /2/, Byfors /3/ and Pfefferle /4/ were used. Results from the calculations are shown in section 2.4.

The modelling of thermal stresses with the creep compliance method, (where total deformations are considered), appears to be somewhat more suitable for numerical analysis than the creep coefficient method.

However, both methods have individual merits. The results of theoretical calculations, using both the creep coefficient and creep compliance method, are therefore presented in this paper.

2.4 Results from theoretical calculations

An example of theoretical calculations of uniaxial thermal stresses with Eqs (2.3) and (2.12) are shown in Fig 2.6. In the calculations, theories for creep in concrete proposed by Bazant /5/, Wilson /7/ (Creep compliance functions), Bernander /2/, Byfors /3/ and Pfefferle /4/ (Creep coefficient functions) have been used.

Fig 2.6 shows a clear discrepancy between the results obtained with different theoretical creep models. However, the same qualitative shapes of the curves are obtained for tensile stresses 4 - 9 days after casting of the structure, and failure occurs according to most of the theories approximately 12 - 16 days after pouring of the concrete specimen.

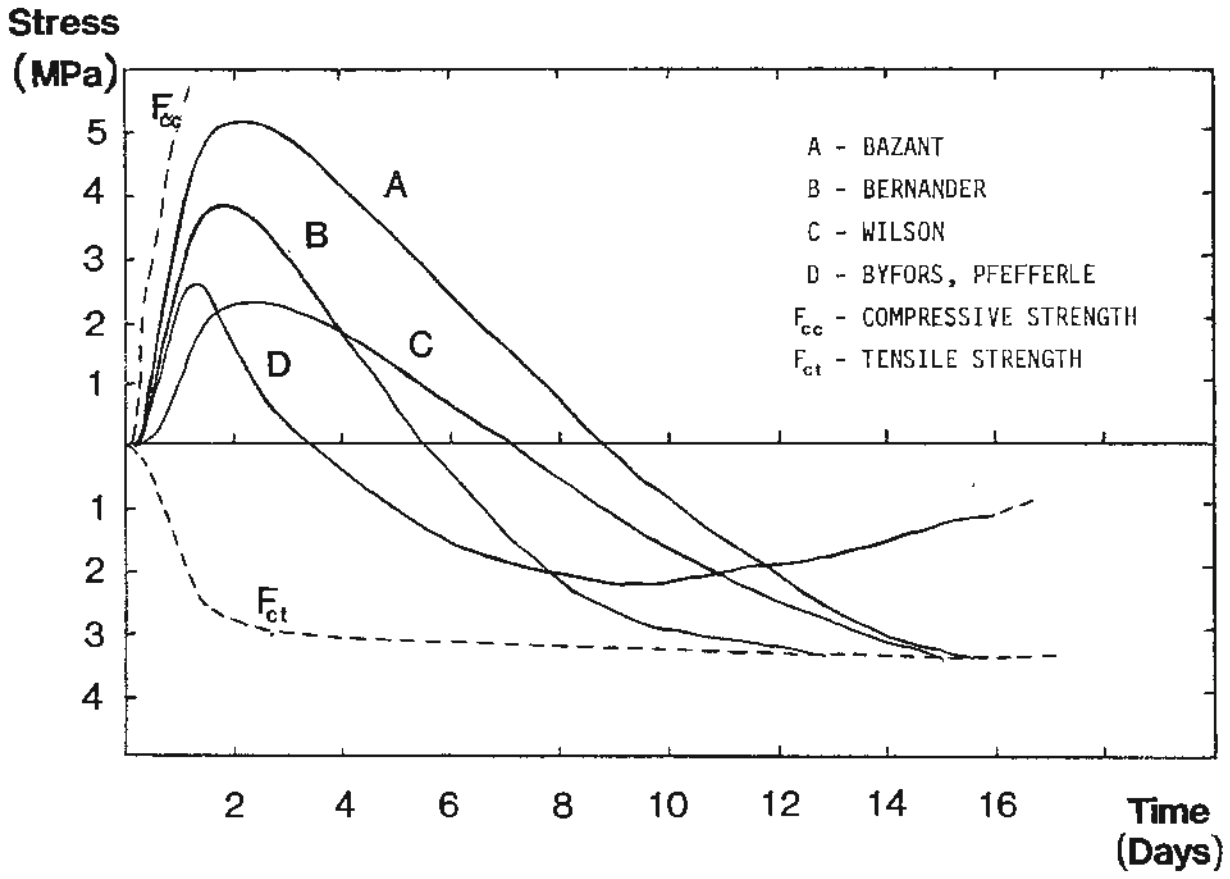

Fig 2.6 Stress-time graphs in a 100 % restrained concrete wall, 2 m thick. Mean temperature rise ΔT_m = 25°C. Concrete: Std, portland, cement content 350 kg/m^3, W/c ratio = 0.53.

3. LABORATORY TESTS

3.1 General

In the laboratory tests, the theoretical models presented in chapter 2 are tested and calibrated for different types of cement, temperature curves, restraints etc.

In the tests, a concrete specimen is placed in a water tank in a servohydraulic testing machine immediately after casting. The concrete is then heated by the surrounding water to give a hydration temperature curve representative for a massive concrete structure. The ends of the specimen are held fixed during the test. This simulates the 100 per cent restraint. The

compressive and tensile forces induced in the specimen are recorded in a load cell. The time when tensile fracture occurs is also determined.

Thus, with the test method described above, different conditions in the production of massive concrete structures can be simulated. Therefore the test method can reduce the need for complicated and expensive full scale field tests.

3.2 Test set-up

The design of the concrete specimen used in the tests is shown in Fig 3.1. The concrete to be tested is situated in the central part of the specimen. A high strength concrete, (e.g. a concrete treated with an accelerating additive), is cast above and below the concrete to be tested. The high strength concrete reduces the deformation and the risk of failure in the connecting zones. The test concrete and the high strength concrete are cast "wet to wet" to give optimum bonding.

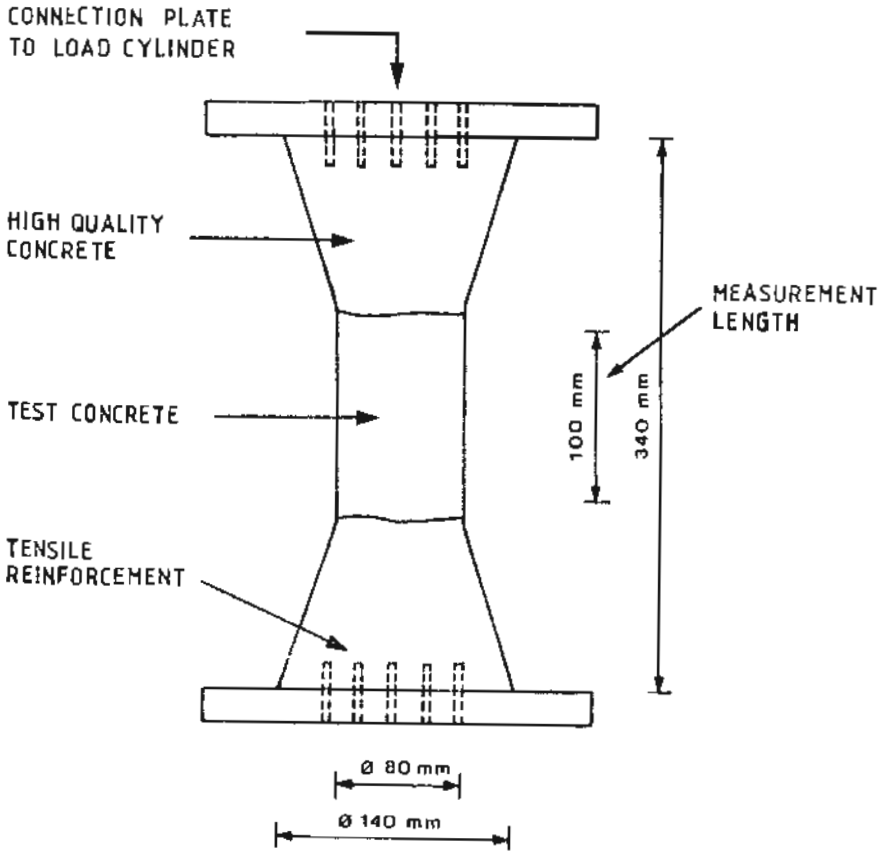

Fig 3.1 Design of test specimen.

Fig 3.2 shows the test set-up with the specimen, the water tank for heating the concrete, the load-cylinder and the electronic control equipment. The heating of the water, the automatic control of the deformations, the loads in the specimen, and the recording of test data are performed by a microcomputer.

To obtain a controlled and purely monotonic loading of the very young concrete, high precision in recording deformation is necessary. For instance, with an inflexible support, a loading or unloading of the specimen will occur if the change of deformation of the concrete exceeds 0.15 µm. Thus long-time stability and accuracy of the gauges as well as adequate stiffness and symmetry of the loading unit is required.

Details of the test set-up with gauges for measurements of the deformation of the concrete is shown in Fig 3.3. Inductive gauges mounted on invar/graphite bars were used for this purpose.

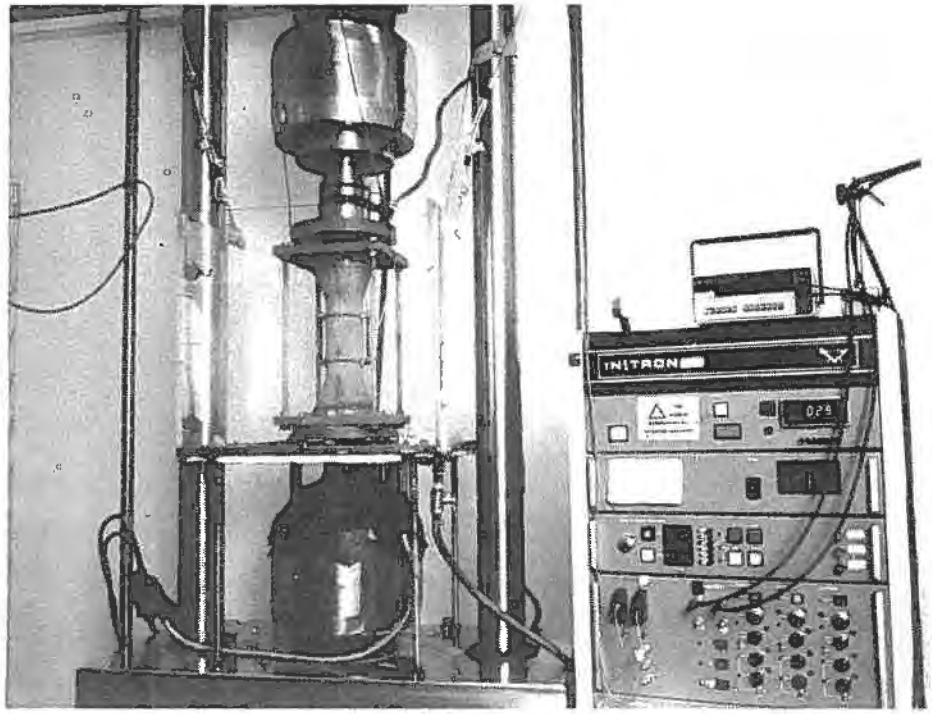

Fig 3.2 Test set-up

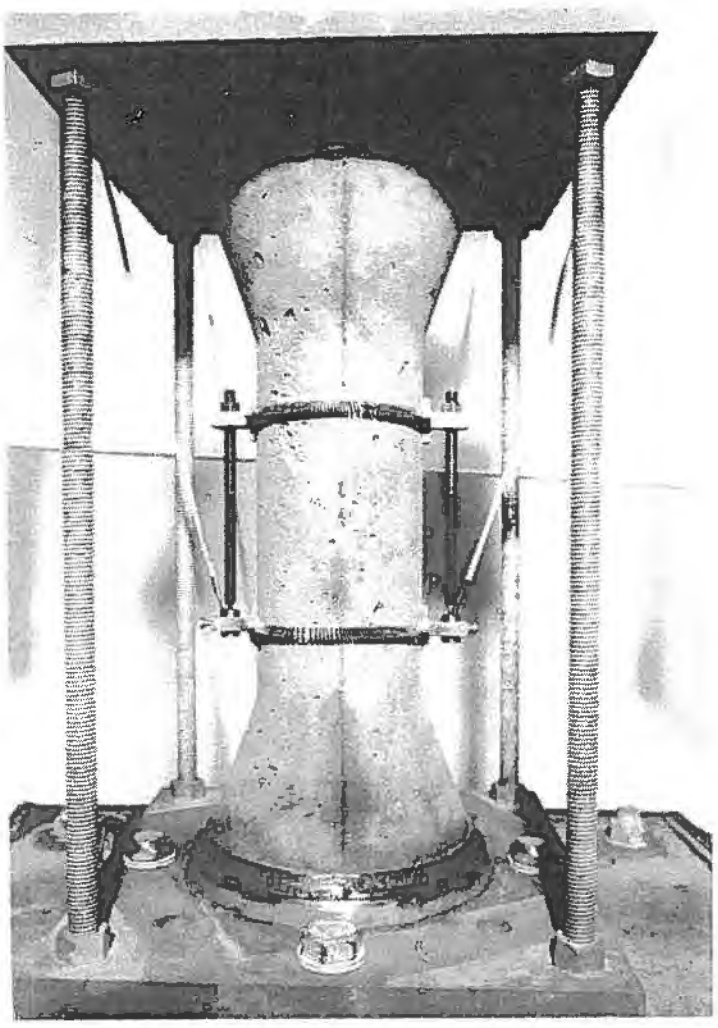

Fig 3.3 Test set-up: Concrete specimen with deformation gauges.

A more detailed description of the test method is given in /8/.

3.3 Test results

The aim of the tests performed was to calibrate and register the response of the concrete for different types of cements, temperature curves, restraints etc. So far, only tests with 100 per cent restraint have been carried out. Some results from these tests are presented here.

Fig 3.4 shows the evolution of thermally induced stresses in an ageing concrete. In this pilot test the temperature curve had a linear shape during the heating with a maximum temperature after

24 hours. During the heating of the concrete inelastic deformation, induced by the creep mechanism of the very young concrete, is obtained. When the concrete cools down, the reduced creep disposition of the concrete induces tensile stresses. Some theoretical calculations and comparison with experimental results are also shown in the figure.

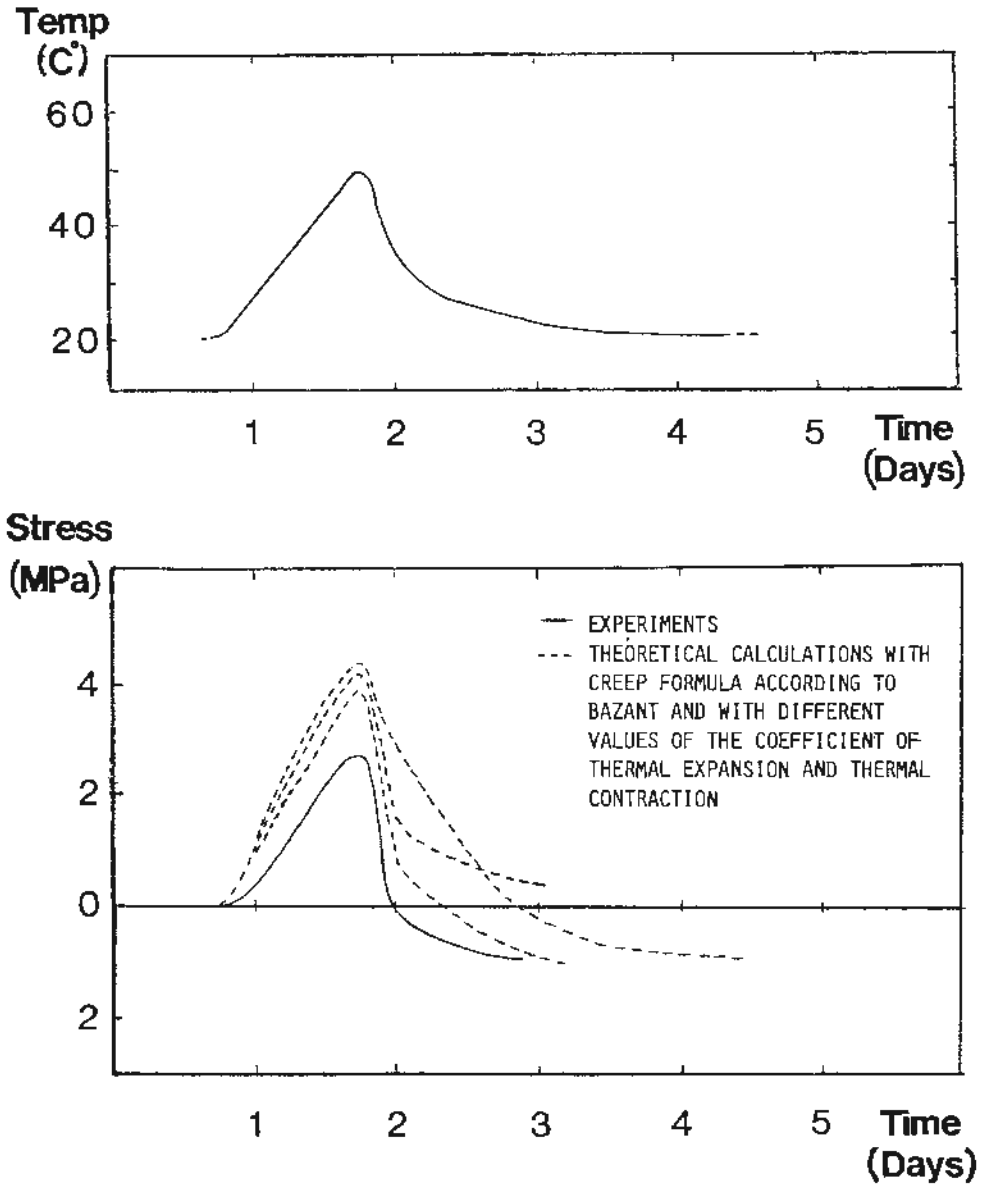

Fig 3.4 Temperature-time and stress-time graphs in a pilot test. The concrete mix composition: Swedish standard portland cement (340 kg/m^3), water (180 l/m^3), sand (990 kg/m^3) and gravel (860 kg/m^3). Theoretical calculations with different creep formulae are also shown.

Fig 3.5 shows the temperature curve from measurements in a 2 m thick wall and the corresponding stress development at 100 per cent restraint obtained in laboratory tests and theoretical calculations. Although the temperature fall in the latter phase of the test is very slow, tensile stresses develop approximately 5 - 12 days after casting. The figure shows that in this case the creep theory according to Bernander renders the best agreement with the test results during the heating of the concrete, while Bazants creep compliance function shows the best agreement with the results in the cooling phase.

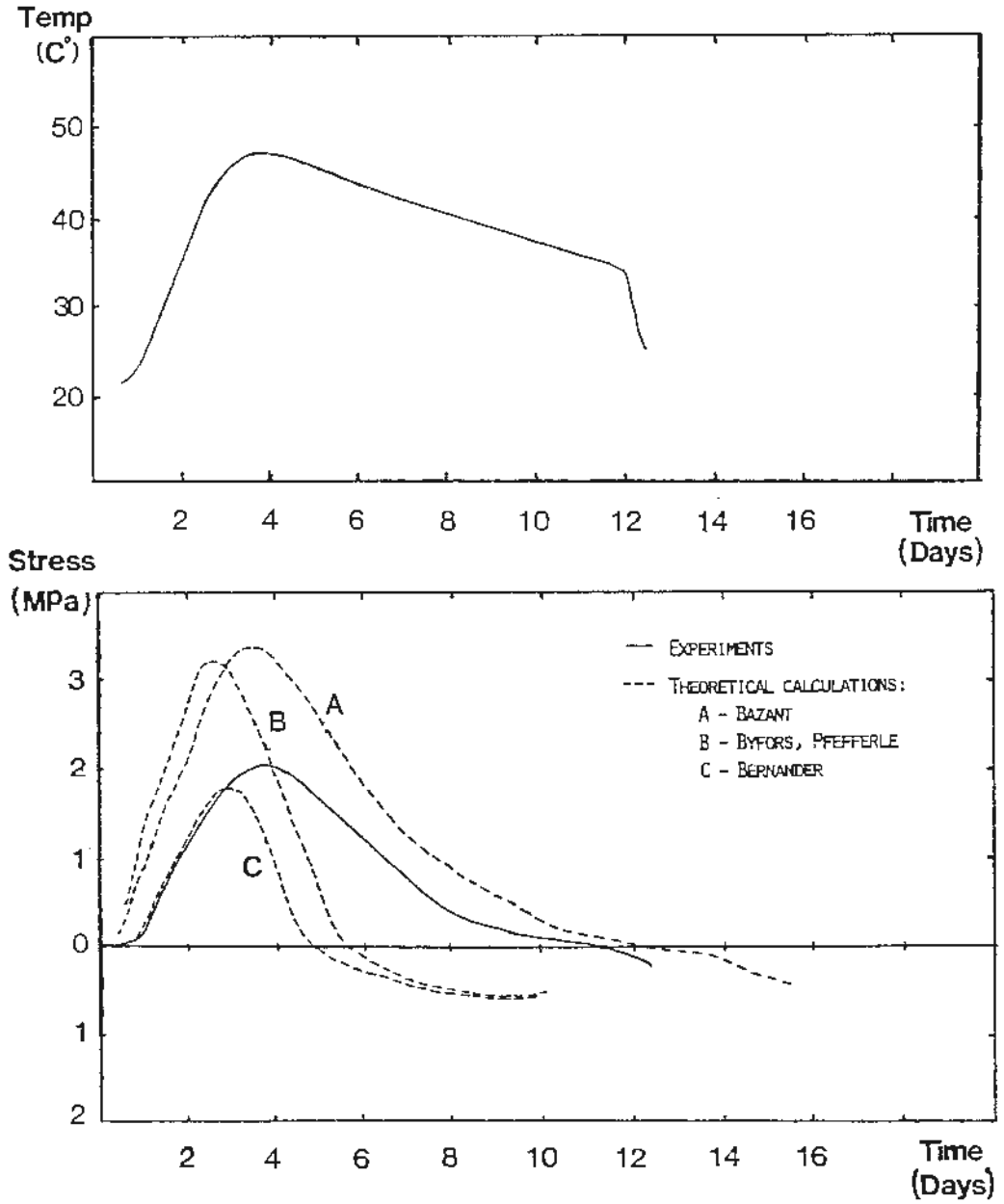

Fig 3.5 Temperature-time graph in a 2 m thick wall and stress-time graphs obtained from tests and theoretical calculations at 100 % restraint. The concrete mix composition is given in Fig 3.4.

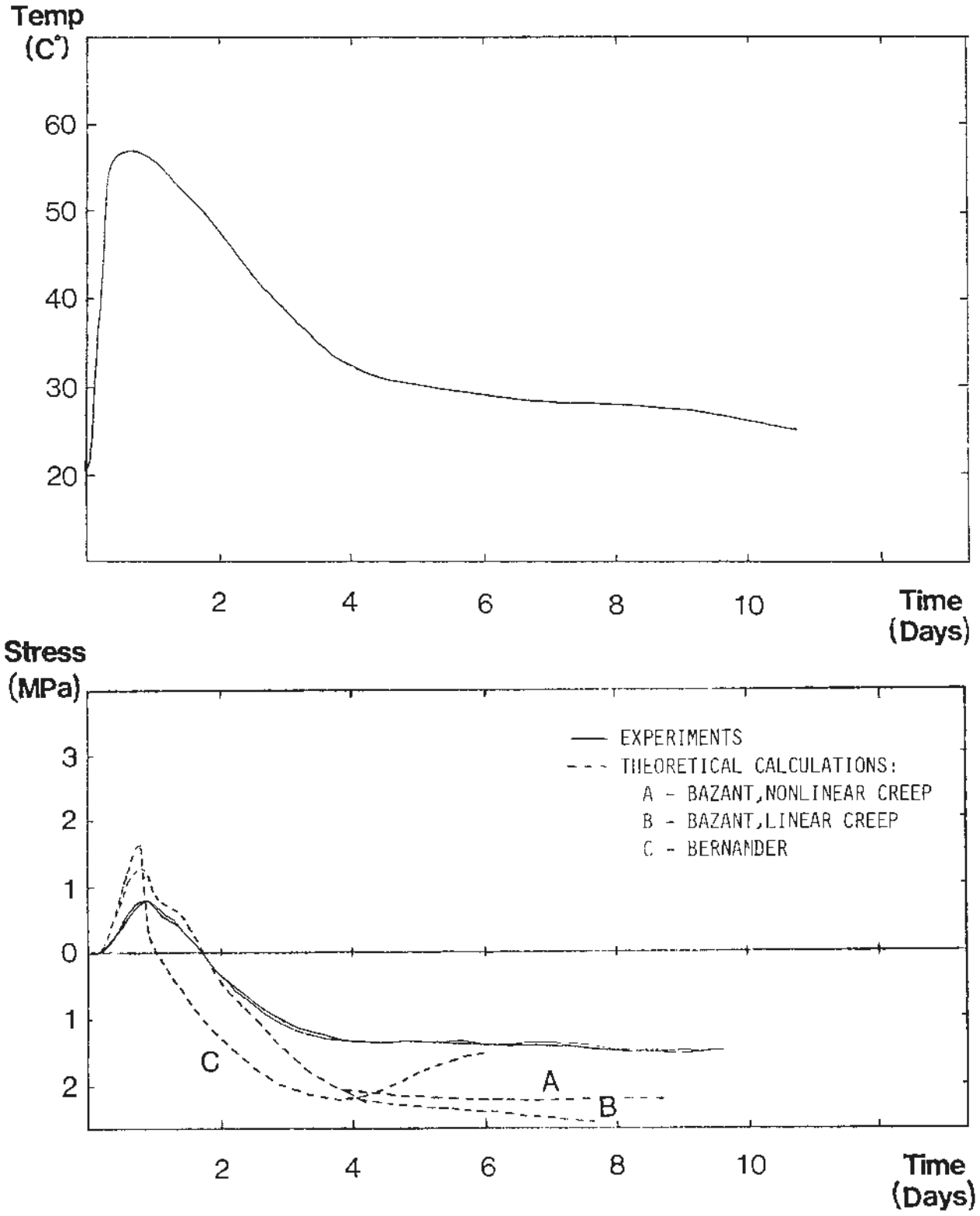

Fig 3.6 Temperature-time graph obtained from in-situ measurements in a 0.7 m thick and 12 m long wall section at Ringhals, Sweden, 1983 /9/. Stress-time graphs from tests and theoretical calculations at 100 per cent restraint are also shown. The concrete mix composition is given in Fig 3.4.

Fig 3.6 shows a temperature curve in a 0.7 m thick wall and corresponding stress development obtained from tests and calculations at 100 % restraint. The temperature measurements were conducted in a full-scale test in which also deformations, crack propagation, temperature rise etc in 12 m long wall sections were studied /9/. We see from Fig 3.6 that the stress-time graphs obtained from two different laboratory experiments using the temperature curve from one of the full-scale field tests show very good agreement with each other. On the other hand (see Fig 3.6) the test results and theoretical curves based on different creep functions differ considerably.

Using the method outlined here, it seems possible to make further studies on the suitability of different creep and compliance functions, and adjust the parameters in the functions selected so that they as correctly as possible model different kinds of concrete.

ACKNOWLEDGEMENT

This investigation is supported by the Swedish Council for Building Research, the Swedish National Road Administration, the Swedish State Power Board and Cementa AB. Hans-Olof Johansson, Laboratory Engineer, conducted most of the laboratory work. Professor Krister Cederwall and Lennart Elfgren, past and present Heads of the Division of Structural Engineering, have provided guidance and constructive criticism.

REFERENCES

/1/ Emborg M: Constitutive models for calculation of viscoelastic temperature stresses in mass concrete. Division of Structural Engineering, Luleå University of Technology, Research Report TULEA 1984:55T, Luleå 1984, (to be published).

/2/ Bernander S, Gustafsson S: Egenspänningar i ung betong p g a temperaturförlopp under hydratationen (Temperature stresses in early age concrete due to hydration, English edition available). Nordisk Betong, No 2, 1981, Stockholm 1981, pp 25-31.

/3/ Byfors J: Plain concrete at early ages. Swedish Cement and Concrete Research Institute, Fo 3:80.

/4/ Pfefferle R: Das Kriechen des Betons, eine Kritisch gedämpfte Schwingung. Beton- und Stahlbetonbau 12, 1979, pp 296-301.

/5/ Bazant Z P: Mathematical models for creep and shrinkage of concrete, chapter 7 in "Creep and shrinkage in concrete structures", edited by Bazant Z P and Wittman F H, Wiley & Sons, New York 1982, pp 163-256.

/6/ Bazant Z P, Panula L: Practical predictions of time-dependent deformations of concrete. Materials and Structures vol II, 1978 (Part I-IV), 307-316, 317-328, 415-423, 424-434, Vol 12, 1979 (Part V-VI), 169-174, 175-183.

/7/ Wilson R: Further development of the Imposed Dischinger Method. Division of Concrete Structures, Chalmers University of Technology, Gothenburg, 1982.

/8/ Emborg M, Johansson H-O: Relaxationsförsök på ung betong (Relaxation test on young concrete, in Swedish with English summary). Division of Structural Engineering, Luleå University of Technology, 1984, (to be published).

/9/ Jansson S, Fagerlund G: Anläggningscement i fullskaleförsök vid Ringhals (Low Alkali, Sulfate Resistant Portlandcement in full-scale test at Ringhals, in Swedish), Cementa No 4, Stockholm 1983, p 6-11.

/10/ Dischinger F: Elastische und plastische Verformungen der Eisenbetontragverke. Der Bauingenieur (Berlin), Vol 20 (1939), Nos 5/6, 21/22, 31/32, 47/48, pp 53-56, 286-294, 426-437, 563-572.

/11/ Cederwall K: Time dependent behaviour of reinforced concrete structures. National Swedish Building Research, Stockholm, Document D3:1971, 173 p.

/12/ Dilger W H: Methods of structural creep analysis, chapter 9 in "Creep and shrinkage in concrete structures", edited by Bazant Z P and Wittman F H, Wiley & Sons, New York 1982, pp 305-339.